Agricultural and Forest Meteorology 350 (2024) 109995

Contents lists available at ScienceDirect

Agricultural and Forest Meteorology

journal homepage: www.elsevier.com/locate/agrformet

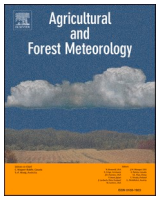

Revealing fine-scale variability in boreal forest temperatures using a mechanistic microclimate model

Joonas Kolstela [a,*], Tuomas Aakala [b], Ilya Maclean [c], Pekka Niittynen [d,e], Julia Kemppinen [f], Miska Luoto [e], Tuuli Rissanen [e], Vilna Tyystjärvi [g], Hilppa Gregow [a], Olli Vapalahti [h,i,j], Juha Aalto [a,e]

[a] Weather and Climate Change Impact Research Unit, Finnish Meteorological Institute, P.O. Box 503, Helsinki FI-00101, Finland
[b] Faculty of Science and Forestry, School of Forest Sciences, University of Eastern Finland, Box 111, FI-80101 Joensuu, Finland
[c] Environment & Sustainability institute, University of Exeter Penryn campus, Penryn, TR10 9FE, United Kingdom
[d] Department of Biological and environmental Science, University of Jyväskylä, P.O. Box 35 FI-40014, Jyväskylä, Finland
[e] Department of Geosciences and Geography, University of Helsinki, P.O. Box 64, Gustaf Hällströmin katu 2a, Helsinki FI-00014, Finland
[f] The Geography Research Unit, University of Oulu, P.O. Box 8000, Oulu FI-90014, Finland
[g] Climate System Research Unit, Finnish Meteorological Institute, P.O. Box 503, Helsinki FI-00101, Finland
[h] Department of Virology, University of Helsinki, P.O. Box 21, Haartmaninkatu 3 00014, Helsinki, Finland
[i] Department of Veterinary Biosciences, University of Helsinki, Agnes Sjöberginkatu 2 PO. Box 66 00014, Helsinki, Finland
[j] Virology and Immunology, HUSLAB, Helsinki University Hospital, Stenbäckinkatu 9 PO. BOX 100, FI-00029 HUS, Helsinki, Finland

ARTICLE INFO

Keywords:
Near surface temperature
Thermal heterogeneity
Forest canopy: Forest microclimate

ABSTRACT

Fine-scale temperatures are important drivers of ecosystem functions and biodiversity in boreal forests. However, accounting for large thermal variability has been difficult due to the coarse spatiotemporal resolution of climate data that is commonly applied in studies of biodiversity and forest health. Here, we use a mechanistic microclimate model and geospatial environmental and weather data to reveal microclimate temperature variability in a broad macroclimatic gradient in boreal forest environments. We modelled hourly near-surface temperatures (0.15 m above ground) in May-August 2020 over three focus areas located in hemiboreal, southern boreal and northern boreal forest zone in Finland at a spatial resolution of 10 m x 10 m. A comparison against data from 150 microclimate stations showed reasonable agreement (root mean square error [RMSE] 2.9 °C) between the measured and modelled temperatures. RMSE for the three focus areas ranged 2.2 –3.2 °C, and the difference was found to be generally smaller under dense canopies compared to open areas. The modelling revealed substantial thermal variability over the landscapes; for example, seasonal near-surface temperature ranges varied 26.5 °C – 42.9 °C, with the variation being smallest in the hemiboreal landscape with multiple large waterbodies, and largest in southern boreal landscape with large wetland areas. These results demonstrate the great potential of mechanistic microclimate modelling to increase our understanding of the thermal characteristics of various boreal forest environments. Ultimately, high-resolution spatiotemporal microclimate data will permit better understanding of e.g., boreal species distribution under climate and land use change and fine-scale variability in disturbances, including insect pests and forest fires.

1. Introduction

Boreal forests cover 27 % of the global forest areas (FAO. 2020) and provide essential ecosystem services such as raw materials, recreation, cultural benefits (Saarikoski et al., 2015) and climate regulation at both local and global scales (Pohjanmies et al., 2017). For example, estimates of carbon storage in boreal forests and soils range from 367.3 Pg to 1715.8 Pg, which is more than in all tropical biomes (Bradshaw and Warkentin, 2015). Climate change is projected to cause large scale effects on boreal forests, increasing both biotic and abiotic risks to these environments and their carbon stocks (Gonzalez et al., 2010; Venäläinen et al., 2020). The fine-scale variability in climate i.e., microclimate (horizontal distances < ~50–100 m (Bramer et al., 2018)), is a key in understanding the level of these risks e.g., controlling fire danger via soil

* Corresponding author.
E-mail address: joonas.kolstela@fmi.fi (J. Kolstela).

https://doi.org/10.1016/j.agrformet.2024.109995
Received 1 July 2023; Received in revised form 25 March 2024; Accepted 29 March 2024
Available online 9 April 2024

and vegetation moisture (e.g., van Wagner, 1974; Venäläinen and Heikinheimo, 2003) and the loss of climatic microrefugia of forest species (Määttänen et al., 2023). However, conventional gridded climate data have coarse spatial resolution ranging from tens to hundreds of kilometers (e.g., ERA5 31×31 km spatial resolution). It is widely known that local climate can vary greatly within small spatial extents with important ecosystem implications (Lembrechts et al., 2019; Lenoir et al., 2013; Aalto et al., 2022).

In the boreal forests, trees dampen, i.e., buffer extreme temperatures between forested and open areas (De Frenne et al., 2019; Gril et al., 2023). Forests also lower the local wind speeds below the canopy and maintain higher relative humidity, and these effects vary even between different tree species (Renaud et al., 2011). Tree canopies absorb and release heat during diurnal cycles, and reflect and absorb radiation, thus reducing the amount reaching the ground (Yuan et al., 2017). Variation in local topography also creates local microclimates e.g., due to equatorward-facing slopes absorbing a higher flux density of shortwave radiation (Geiger, 1965). Water bodies may also mediate local climate variability for instance via a buffering effect on the surrounding area and leading to increased precipitation (Samuelsson et al., 2010; Aalto et al., 2016). While these local effects are well known, measurements and spatiotemporal estimates of microclimates at larger extents have been so far limited.

Advancements in microclimate measuring devices (e.g., Wild et al., 2019) have made collecting microclimate data more practical and affordable than before. This has opened new avenues for microclimate research, both on a small and large spatiotemporal scale (Lembrechts et al., 2020). Such measurement systems help in advancing our understanding of the range of microclimatic conditions, but they still only depict the variability at the measurement site. Empirical microclimate models are computationally efficient and can provide reliable results within the original measurement area, but their quality can quickly deteriorate when attempting to extrapolate values outside the area and data used for model fitting (Kemppinen et al., 2023).

However, recently, mechanistic microclimate models have begun to emerge. These models, such as *NichemapR* (Kearney et al., 2017) and *microclimc* (Maclean et al., 2021a) (based on the models developed by Porter et al., [1973] and Goudriaan and Waggoner [1972], respectively), are based on principles of energy balance, namely radiative, sensible, and latent heat fluxes for a single point-location. A new addition to the list of mechanistic models is the spatially-resolved *microclimf* model (Maclean and Klinges, 2023). With a set of input variables depicting weather parameters, vegetation, and topography, this type of mechanistic model allows the creation of spatiotemporal microclimate data at high resolution to any time and location. The model has previously been tested only over a single km square area of Great-Britain and thus has not previously been applied in a boreal forest environment, where the varying forest types, large amounts of waterbodies and varying topography are expected to lead to a wide range of microclimate conditions. With a recent large microclimate dataset collected in Finland (Aalto et al., 2022) the *microclimf* model can now be thoroughly tested for these environments. With regards to this, we aim to (1) test the applicability of the *microclimf* model for generating high temporal (hourly) and spatial (10 m x 10 m) resolution microclimate data in boreal forests, and (2) investigate the model's predictive performance in respect to the environmental conditions. Our study is grounded on three different boreal forest areas in Finland and a large microclimate station network that allows for rigorous comparison between model outputs and the observations.

2. Material and methods

2.1. Study area

The study setting consists of three focus areas located in Finland and across different forest vegetation zones. These focus areas were selected due to the available microclimatic measurement data (Aalto et al., 2022). The focus areas are in hemiboreal Karkali (KAR; lat 60.24, lon 23.79; area ca. 47.5 km^2), southern boreal Hyytiälä (HYY; lat 61.82, lon 24.15, ca. 51.5 km^2), and northern boreal Värriö (VAR; lat 67.73, lon 29.56, ca. 22.7 km^2) (Fig. 1). Each of these areas has different characteristics and variation in terms of topography, vegetation, and land cover, providing unique model testing environments (Table 1).

The southernmost area, KAR, contains both deciduous and coniferous trees. Of the three focus areas, it contains the highest amount of tree biomass and canopy coverage, while the local agricultural fields lead to many edge areas between forests and open areas. A defining feature is the large waterbody (lake Lohjanjärvi) covering most of the focus area, along with several smaller ponds. The midmost area, HYY, has similar amounts of biomass and canopy coverage as KAR. Here, the defining features are the large mires. Vegetation consists of mixed deciduous and coniferous forests. In the north, VAR has the lowest amount of biomass and canopy cover and largest variation in elevation, as it has multiple valleys and fell tops. Vegetation consists of coniferous forests, downy birch forests, and open tundra on the highest fell tops above the tree line.

2.1.1. Microclimate measurements

Each focus area contained 50 – 55 microclimate logger sites, each containing a Tomst TMS-4 (Wild et al., 2019). The Tomst loggers measure at 15-minute interval temperatures at 2 cm and 15 cm above ground (precision of 0.0625 °C and accuracy of ± 0.50 °C). In this study, we used the 15 cm above-ground temperature values from 1.5.2020 – 31.8.2020 for validating the model results for each of the three chosen focus areas. An exemption to this is the values from the VAR focus area, from which we used values from 10.6.2020 – 31.8.2020 due to snow that covered most of the measurement sites until then. This height was chosen due to the known large variability in microclimatic temperatures near the ground layer and its relevance to many ground-dwelling organisms and surface conditions.

2.2. Mechanistic microclimate model

Our study used the open-source mechanistic microclimate model *microclimf* (Maclean and Klinges, 2023), version 0.1.0, developed for the R software environment (R core team 2023). The model is part of a family of mechanistic microclimate models (the others being *microclima* [Maclean et al., 2019] and *microclimc* [Maclean and Klinges, 2021a]). The *microclimf* package contains tools for data processing, editing, and finally, creating microclimate data at an hourly or daily temporal resolution. Spatial resolution is defined by the resolution of the vegetation and terrain data provided as inputs to the model. Model outputs are produced at above or below ground, or within or below the forest canopy layer at the requested height. Output variables consist of temperature at the requested height, ground-surface and leaves, soil moisture fraction in the upper soil layer, relative humidity, wind speed, and direct, diffuse, and longwave radiation fluxes (Maclean and Klinges, 2023).

The *microclimf* model is a modified version of the *microclimc* model, which was designed for creating microclimate data and differs principally in (1) being designed for computational efficiency so that it can be applied across landscapes and (2) incorporated an emulator of Raupach's (1987) localized near-field model for quantifying heat and vapor transfer below canopy. The first step of modelling is to apply the Dickinson et al. (1986) two-stream approximation model to estimate canopy albedo and radiation absorbed by the ground. In deriving microclimate above canopy, or (following Ogée et al., 2003) as initial step when deriving microclimate below canopy, the vegetation layer is then treated as a 'bigleaf' - namely a single layer of phytomass without vertical structure and the height and leaf area of the vegetation is used to derive roughness lengths for heat and momentum using the method detailed in Raupach 1994. The energy balance of the canopy and ground surface is

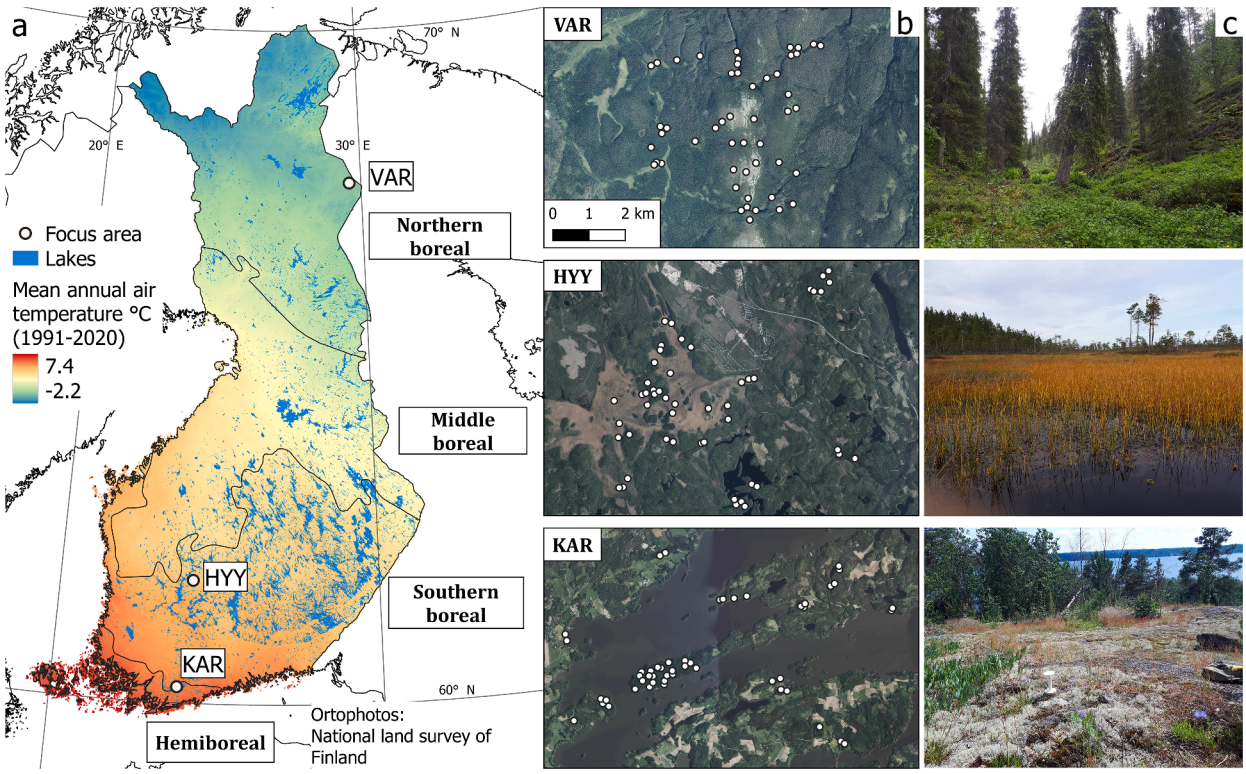

Fig. 1. The three focus areas in Finland. KAR (Karkali) in the hemiboreal, HYY (Hyytiälä) in the southern boreal, and VAR (Värriö) in the northern boreal area are presented in panel a. Focus areas and microclimate measurement sites have been marked in panel b, and on panel c is an example photograph from each of the areas. Photos: Pekka Niittynen 2020. Mean annual air temperature from Jokinen et al. (2021).

Table 1
Variation in the environmental data: 1st, 25th, 50th, 75th and 99th percentiles for the DEM (Digital Elevation Model), slope, PAI (Plant Area Index), tree height, canopy cover and TPI-500 (Topographic Position Index, 500 m radius) variables. Values have been calculated for the KAR (Karkali), HYY (Hyytiälä) and VAR (Värriö) areas. DEM, slope, PAI, tree height and tpi-500 have been calculated from light detection and ranging (LiDAR) data provided by the National Land Survey of Finland (NLS) and the canopy cover and biomass have been calculated from Natural Resources Institute Finland datasets. Biomass is the sum of the different parts of spruce, pine, and deciduous trees biomass.

KAR	1st percentile	25th percentile	50th percentile	75th percentile	99th percentile
DEM (m)	31.9	32.2	34.3	52.0	81.0
slope (degrees)	0.2	2.5	5.1	9.2	27.3
PAI	0.0	0.2	1.0	1.9	5.3
tree height (m)	0.0	4.5	14.5	20.4	30.1
canopy cover (%)	9.9	56.0	68.0	74.4	84.9
tpi-500	−13.2	−3.5	−0.6	1.8	19.9
biomass (10 kg/ha)	358.2	8224.0	12,698.6	16,811.1	26,732.8
HYY	1st percentile	25th percentile	50th percentile	75th percentile	99th percentile
DEM (m)	152.0	167.5	170.5	175.1	198.8
slope (degrees)	0.1	0.6	2.1	5.3	18.6
PAI	0.0	0.0	0.6	1.2	3.5
tree height (m)	0.0	4.1	13.4	18.2	27.3
canopy cover (%)	0.0	31.2	61.6	71.2	85.2
tpi-500	−8.3	−2.2	−0.4	1.6	11.7
biomass (10 kg/ha)	0.0	3377.7	9741.9	13,245.7	22,813.5
VAR	1st percentile	25th percentile	50th percentile	75th percentile	99th percentile
DEM (m)	221.2	279.9	306.5	353.0	468.0
slope (degrees)	0.2	1.7	3.3	6.0	27.3
PAI	0.0	0.1	0.2	0.4	1.2
tree height (m)	0.0	6.7	12.1	16.2	22.0
canopy cover (%)	0.1	29.6	36.7	43.7	61.4
tpi-500	−21.4	−3.3	−0.3	3.0	22.8
biomass (10 kg/ha)	0.0	3598.4	5057.3	6447.3	9519.6

then solved using the Penman-Monteith equation (Penman1948; Monteith 1965) to derive temperature and effective vapor pressure at the soil surface and at the top of the canopy. Following Harman and Finnigan (2007) it is then assumed that in dense canopies both wind speed and heat flux profiles decline exponentially from the top of the canopy owing to similar absorption of both radiation and momentum by

canopy foliage. In consequence, the far-field temperature and vapor profiles, independent of the underlying ground layer, become approximately linear and can be derived by solving the energy budget for the entire canopy. The non-diffusive 'near-field' contribution is assumed to be influenced most strongly by local source concentration and is thus determined from foliage density and the net energy balance of canopy elements at the height specified by the user. In so doing, a vertical profile of foliage is simulated and minor empirically-derived adjustment to account for variation in wind speed and canopy height. In this way, air and leaf temperature and air relative humidity at any user-specified height below the canopy can be derived in a computationally efficient manner without the need to run a full multi-layer canopy model.

2.3. Model input data

2.3.1. Meteorological forcing

The used meteorological forcing data consists of temperature, relative humidity, sky emissivity, wind speed and direction, shortwave, and diffuse radiation at a temporal resolution of one hour, and daily precipitation. Weather data was collected from two sources: 1) The Finnish Meteorological Institute's (FMI) Climgrid database (Aalto et al., 2016), and 2) the ERA5 reanalysis dataset by the European Centre of Medium-Range Weather Forecasts (ECMWF) using the *mcera5* package (Klinges et al., 2022). Temperature, relative humidity, and daily precipitation values were extracted from the FMI climgrid database due to its higher spatial resolution, validated interpolation methodology, and it being based on the quality controlled national measurement network weather data. The values are from the following hours: 00:00, 03:00, 06:00, 09:00, 12:00, 15:00, 18:00, and 21:00. Sky emissivity, wind speed and direction, shortwave and diffuse radiation were extracted from the ERA5, for which the necessary format transformations and interpolations were done using the microctools package (Maclean and Klinges, 2023). The spatial resolution of these datasets is 10 km x 10 km grid for the FMI climgrid database and ERA5 31×31 km. ERA5 data is at an hourly temporal resolution and the FMI climgrid is at a three-hour temporal resolution, from which the temperature and relative humidity values were interpolated to hourly resolution using linear interpolation in the *approxfun* function of the stats package in R (R Core team 2023).

2.3.2. Geospatial environmental data

The spatial data used depicts vegetation properties and structure, and topography. Vegetation information consists of Plant Area Index (PAI), tree heights, ratios of vertical to horizontal projections of leaf foliage, maximum stomatal conductance values, canopy clumpiness, leaf reflectance and transmittance values for shortwave radiation and leaf diameter information. We used light detection and ranging (LiDAR) data provided by the National Land Survey of Finland (NLS) to calculate the PAI, and tree height values for the focus area. PAI values were calculated in Python using *ALS2PAD* software (Arnqvist et al., 2020). The NLS LiDAR data is openly available data with a point density of 0.5 p/m^2, which has been collected during the leaf-on period. We acknowledge the fairly low point density of the data which may cause uncertainty in deriving vegetation structure variables. However, the data was chosen due to the lack of alternative high-precision LiDAR datasets from these focus areas. The potential effects on results due to this data are discussed further in the discussion section.

Ratios of vertical to horizontal projections of leaf foliage, maximum stomatal conductance values, canopy clumpiness, leaf reflectance and transmittance values for shortwave radiation and leaf diameter information were all generated using the *vegpfromhab* function provided in the *microclimf* model. The function uses the habitat type, PAI, and vegetation height information to generate these values based on MODIS-derived estimates (Maclean and Klinges, 2023). The topography data consists of the area's Digital Elevation Model (DEM), which was also calculated from the LiDAR data. Soil information consists of soil type and their shortwave radiation reflectance values. Due to a lack of a dataset of soil types at a reasonably high spatial resolution, in addition to lacking proper parameterization of the different soil types for the model, we decided on using a homogenous value for both the soil type, and its shortwave reflectance value for each area.

2.3.3. Model implementation

Due to the large waterbody in KAR, we used the *waterbody effects* -function (Maclean et al., 2019) to calculate their effects on the temperature values in the area (Fig. 2). Using thin-plate spline interpolation along with three covariates (sea and land temperature differences, coastal exposure in an upwind direction and coastal exposure disregarding wind direction), the function calculates finer resolution temperature data from the coarser reference. On average differences between reference and output temperatures ranged from 0.25 to 0.31°, being higher near the edge of water than further inland in the southern area, while having a cooling effect in the north.

Model runs were done in a supercomputing environment of the CSC (IT center for science) PUHTI system. Due to large computational burden, the model runs were divided into two-day segments. This allowed for running the model on multiple computation nodes, lowering overall run times, and lowering the memory requirements of each of the model runs.

The microclimate model runs resulted in temperature arrays at 0.15 m height for each of the three research areas. These arrays have a temporal resolution of one hour and a spatial resolution of 10 m x 10 m. These results were compared to the available microclimatic observations from the three focus areas. Model outputs were extracted based on the measurement site coordinates, and utilized identical time intervals as the three-hourly climgrid dataset. We calculated the Root Mean Square Error (RMSE), Pearson Correlation (r), coefficient of determination (R^2) and bias (modelled values subtracted from measured values) of the measurement and model time series. These values were calculated for the daily maximum, minimum and mean temperatures, in addition to the three-hourly (Table 2) and hourly time-series (Supplementary Table 1) between all measurement sites. We also calculated r and R^2 values between maximum, minimum and temperature ranges and different vegetation and topography variables (Supplementary Table 2). The chosen vegetation variables were PAI, tree height and habitat type and the topography variables were DEM, slope, aspect, and TPI-500 (Topographic Position Index, 500 m radius). The RMSE between measured and modelled temperatures and daily maximum and minimum temperature bias from each site were compared to selected vegetation and topography variables to see if the model performance was affected by them (Supplementary Table 3). Lastly, the measurement sites were divided into a set of environments for comparisons. These environments consisted of forests – openings, level – sloped terrain, North-West – South-East aspects, negative – positive TPI and lastly short – tall trees. RMSE between measured and modelled values, and daily maximum and minimum temperature bias were compared between these different kinds of environments.

3. Results

3.1. Model validation

3.1.1. Overall performance

The three focus areas show large variability in environmental conditions (Table 1). Model validation was done between the measured and modelled near-surface microclimate temperatures at a 15 cm height. In these results, we concentrate on the three-hourly values due to the lack of temporal interpolation, but the RMSE between measured and modelled values and maximum and minimum temperature bias for all values can be found in Supplementary Table 1. The three-hourly values RMSE between all measurements and modelled values from all three areas and times was 2.9 °C, R^2 was 0.79 and temperature bias was −0.5

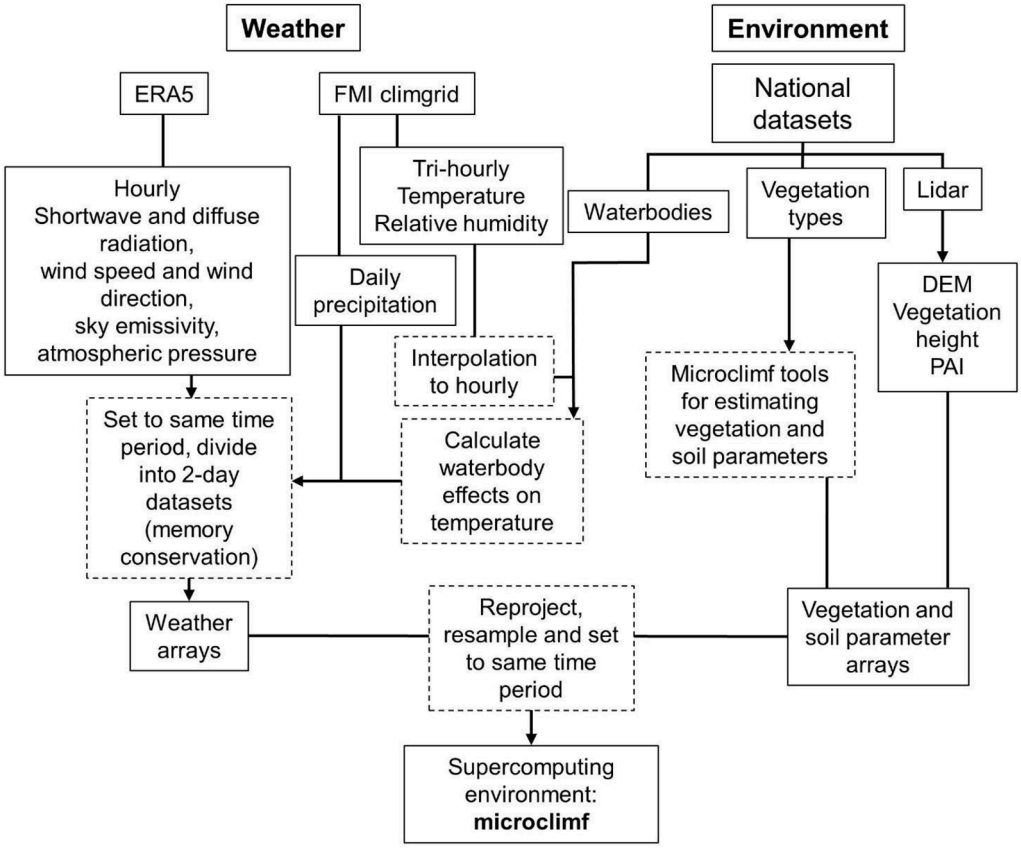

Fig. 2. Workflow of input parameter collection and editing for model runs. Dashed outlines depict data processing phases in the workflow. FMI, Finnish Meteorological Institute. LiDAR, light detection and ranging. DEM, digital elevation model. PAI, plant area index.

Table 2
Root Mean Square Error (RMSE) between measured and modelled temperatures, coefficient of determination (R^2) and bias (modelled values subtracted from measured values) for daily maximum, minimum and mean temperatures (temp), based on the three-hourly values of measured and modelled temperatures at each focus area averaged over all measurement sites. Comparisons for VAR (Värriö) are limited to 10.6 – 31.8 due to snow cover.

	Daily max temp			Daily min temp		
Area	RMSE	R^2	bias	RMSE	R^2	bias
KAR	1.3	0.93	−0.1	0.6	0.98	−0.2
HYY	1.7	0.97	1.3	2.7	0.95	−2.5
VAR	2.5	0.82	1.5	2.1	0.69	−0.8
	Daily mean temp			All measurements		
Area	RMSE	R^2	bias	RMSE	R^2	bias
KAR	0.8	0.98	−0.6	2.2	0.84	−0.6
HYY	1.0	0.99	−0.8	3.2	0.80	−0.8
VAR	0.9	0.92	0.0	3.0	0.72	0.4

°C (Fig. S1). With all measurements and comparing each site separately (Table 2), the KAR area had the lowest RMSE (2.2 °C), and highest R^2 (0.84). HYY had an RMSE of 3.2 °C, and R^2 of 0.80. VAR had an RMSE of 3.0 °C, and R^2 of 0.72. There was a negative temperature bias for KAR (−0.6 °C) and HYY (−0.8 °C), and a positive for VAR (0.4 °C). When comparing values averaged over all sites in each area, KAR also had the lowest RMSE value for the daily maximum (1.3 °C), minimum (0.6 °C) and mean (0.8 °C) temperature comparisons. HYY had the highest RMSE for both the daily minimum temperatures (2.7 °C) and mean temperatures (1.0 °C), while VAR had the highest RMSE for the daily maximum temperatures (2.5 °C). For all areas, R^2 values were high, with VAR minimum temperatures being lowest (0.69). Comparisons between each individual measurement site (Fig. 3) show higher RMSE and lower correlation and coefficient of determination values compared to daily values. Results are otherwise similar as in the values averaged over all sites in each area, with the model performing the best in KAR. Measured and modelled temperature RMSE values ranged from 2.7 to 3.6 °C, being the highest in June. There was a negative temperature bias in all months (−0.4 - −0.6 °C).

3.1.2. *Observed and modelled temperature variability*

Modelled values have smaller temperature ranges than measured values in both daily maximum and minimum values (Fig. 4a) and monthly temperature ranges (Fig. 4b) for each focus area, especially in HYY. Differences were smallest in May and largest in June in KAR and HYY, while the differences in VAR were not found to be statistically significant for any of the months. Both measured and modelled temperatures have higher temperature ranges than ERA5 macroclimate data (Fig. S2), the differences being larger in the daily maximum temperatures than in the minimum temperatures.

3.2. *Models predictive performance in respect to the environmental conditions*

Model results show great temperature variability in each of the areas (Fig. 5). PAI had the strongest effect on maximum temperatures and temperature ranges in each area, followed by tree height (Supplementary Table 2). For minimum temperatures the only variables with a noticeable and significant effect were DEM in KAR and tree height in VAR, although the R^2 values are low (0.15 and 0.07 respectively).

The largest effect on RMSE between measured and modelled temperatures in KAR and HYY was found in the vegetation parameters PAI and tree height, being especially strong in HYY (PAI $r = -0.82$ and $R^2 = 0.66$) (Supplementary Table 3). In VAR the highest effect was from

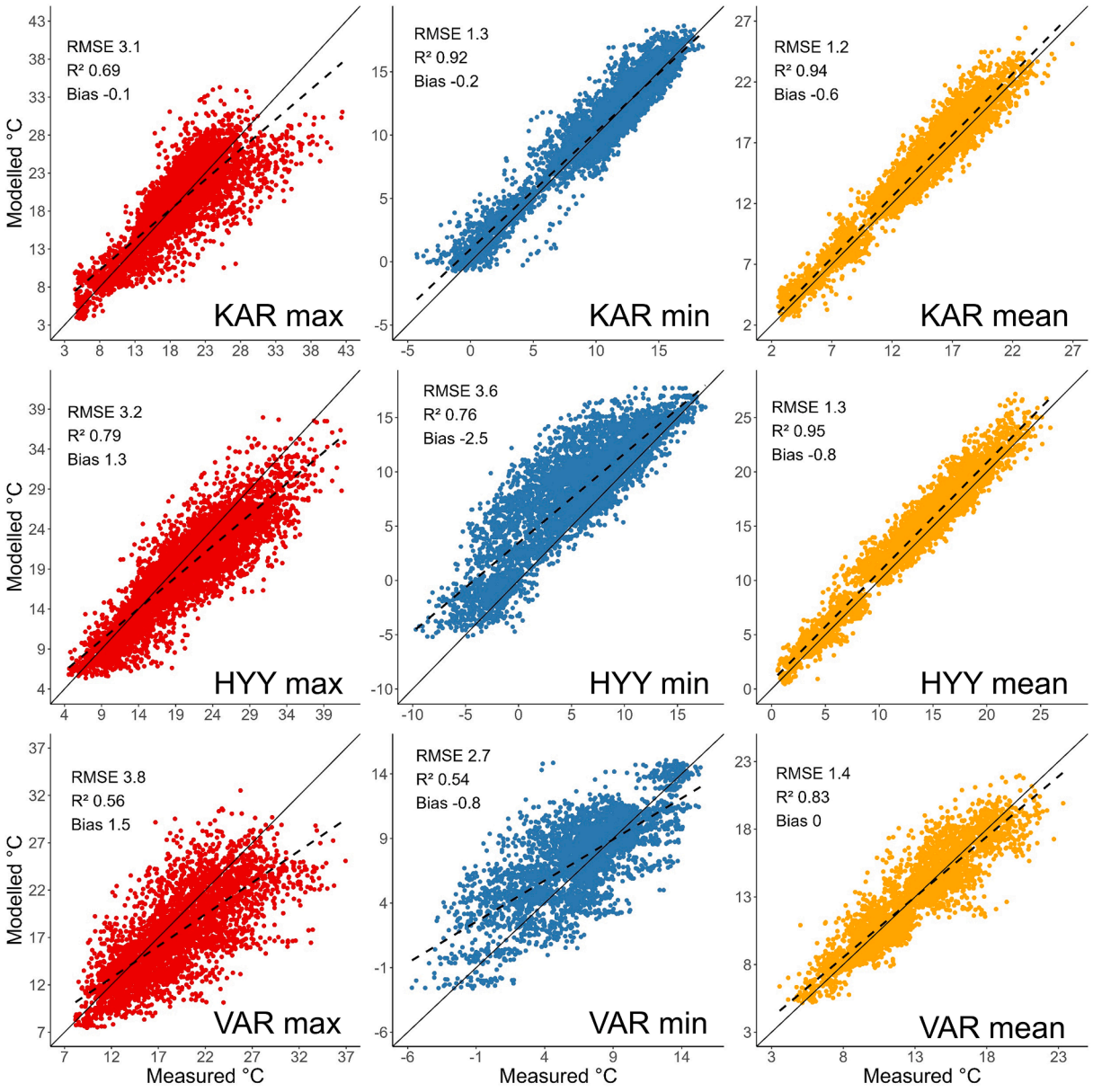

Fig. 3. Comparisons of the KAR (Karkali), HYY (Hyytiälä), and VAR (Värriö) daily measured and modelled maximum (max, red), minimum (min, blue), and mean (orange) temperatures at each individual measurement site based on the three-hourly temperature values. The linear regression line is presented as a dashed black line while the solid black lines depict 1:1. RMSE, Root Mean Square Error. R^2, coefficient of determination.

aspect ($r = -0.42$ and $R^2 = 0.18$). For maximum temperature bias slope and tree height had the greatest effect in KAR and HYY, while only slope had a significant effect in VAR. For minimum temperature bias the only variable with a statistically significant effect was habitat type in HYY and especially VAR ($r = -0.52$ and R^2 0.27).

In general, RMSE between measured and modelled values is lower in more forested areas with taller trees, sloped, North-West facing areas at higher ground (Fig. 6). This was also evident for the daily maximum and minimum temperature bias, where bias was closer to zero in such environments. However, the effect of TPI on maximum temperature bias and tree height and aspect on minimum temperature bias was not statistically significant. Aspect did not have as strong of an effect as the other variables, except for maximum temperature bias.

Largest differences in RMSE of measured and modelled temperatures in KAR were in the short – tall tree environments (Supplementary Table 4), in HYY there were significant differences between all environments except North-West – South-East facing slopes and lastly in VAR overall level of difference was smaller than in KAR and HYY but was evident in each environment comparison. In KAR differences in maximum temperature bias were found between all environments except negative – positive TPI (Supplementary Table 5). In HYY all environments had noticeable differences, the largest being level – sloped environments, and in VAR between North-West – South-East facing slopes. For minimum temperature bias the largest difference in KAR was between short – tall forest environments, in HYY forest – open environments and lastly in VAR negative – positive TPI environments (Supplementary Table 6). It should be noted that there is a large group size difference for the tree height environments in KAR and HYY,

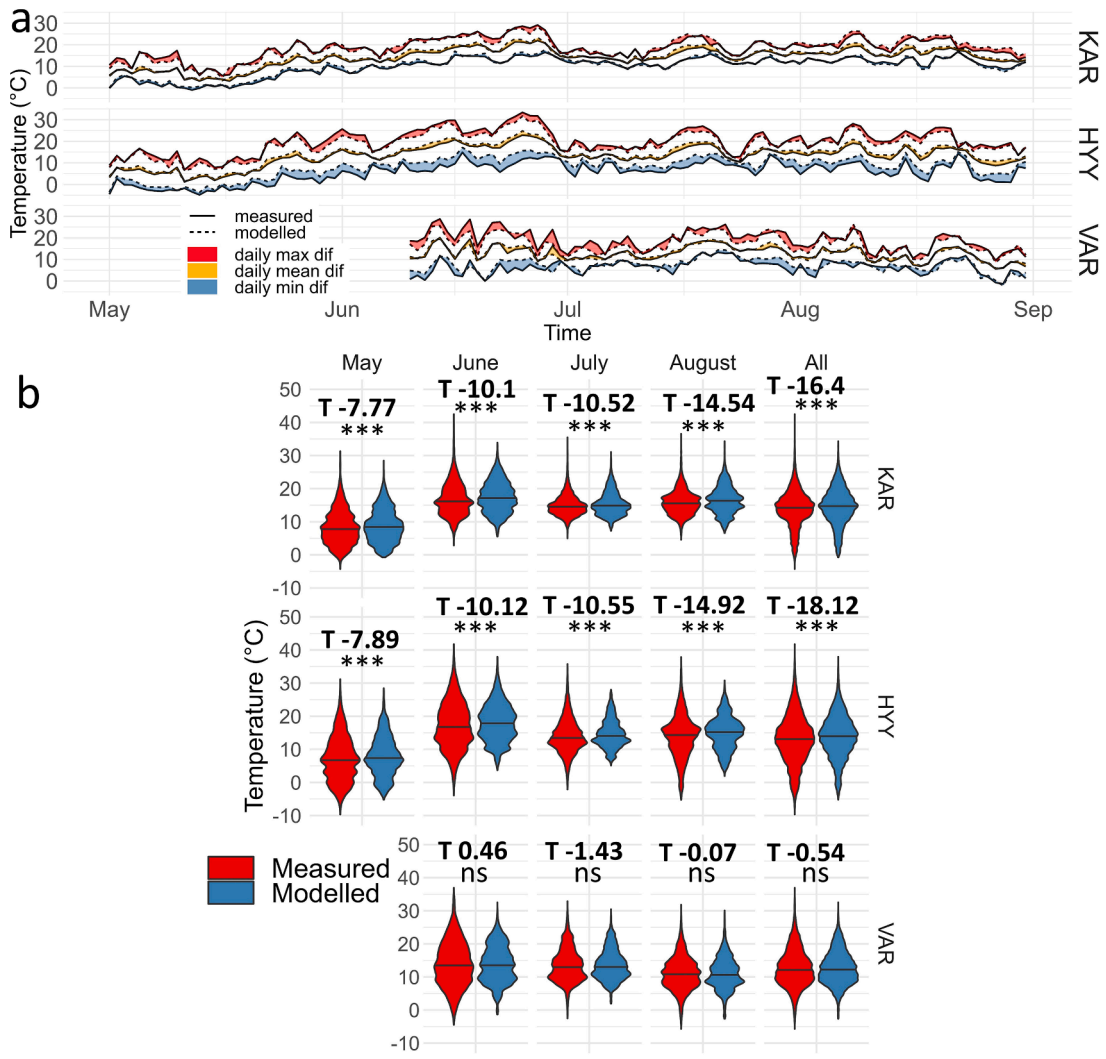

Fig. 4. a) Timeseries of daily maximum, minimum, and mean temperatures of measured and modelled three hourly temperature values, averaged over the three focus areas. dif, difference. b) Three-hourly measured and modelled temperatures over all months, and each month separately in each focus area. Black line depicts the 0.5 quartile. Note that VAR data were available only starting from 10.6.. KAR, Karkali. HYY, Hyytiälä and VAR, Värriö. In figure b) level of significance is depicted as $P < 0.001$ = ***, $P < 0.01$ = **, $P < 0.05$ = * and $P > 0.05$ = ns (not significant), and the T-value of the Welch's T-test is reported as T.

potentially affecting the results.

4. Discussion

4.1. Model performance and its variation in respect to environmental conditions

The model is mostly capable of following the temperature variation within each site, although the variability and temperature ranges of modelled values tend to be suppressed compared to the measured values. Performance was otherwise consistent over the May-August period in each area, except for June. This could be due to the high (almost 4°) temperature anomaly for June compared to May, July, and August of 2020 in Finland (Finnish Meteorological Institute, 2021), potentially causing larger differences in measured and modelled temperature extremes.

In agreement with previous research covering boreal environments, the temperature variability is largely driven by differences in forest canopy (represented by PAI and tree height in this study) (e.g., Aalto et al., 2022; Thom et al., 2020), as is the model performance. This is seen in the hemiboreal area KAR between forests and numerous open areas (agricultural fields), in HYY between forests and the large wetlands and in VAR the forests and open fell tops. Variability is also evident within forested areas, having strong negative correlation with maximum temperatures and PAI and tree height. Here differences in the canopy cover can lead to increased flux densities of shortwave radiation reaching the ground layer compared to the adjacent area.

Model performance varied between the focus areas, KAR having the overall best performance. This could be due to the large temperature buffering waterbodies in the area (Wen et al., 2015), which were captured in the model implementation using the waterbody function. Measurement sites were also located in more forested areas than in HYY and VAR, limiting the maximum temperature bias caused by potential measurement device overheating as discussed in 4.2, methodological limitations. The especially large minimum temperature bias in HYY could be due to an overestimation of the wetlands' high specific heat capacity and ability to reduce outgoing long-wave radiation (Yu and Liu, 2019). The potential overheating of the measurement devices could play a larger role in the prediction error due to many of the sites being in open areas with no canopy cover. This could also be the reason for performance being better in sites with more sloped terrain with positive TPI, as the more level sites with negative TPI are in the open wetland areas. In VAR, elevation differences have a stronger effect on temperatures than in the other areas. Slopes as well as the fell tops can be seen heating up

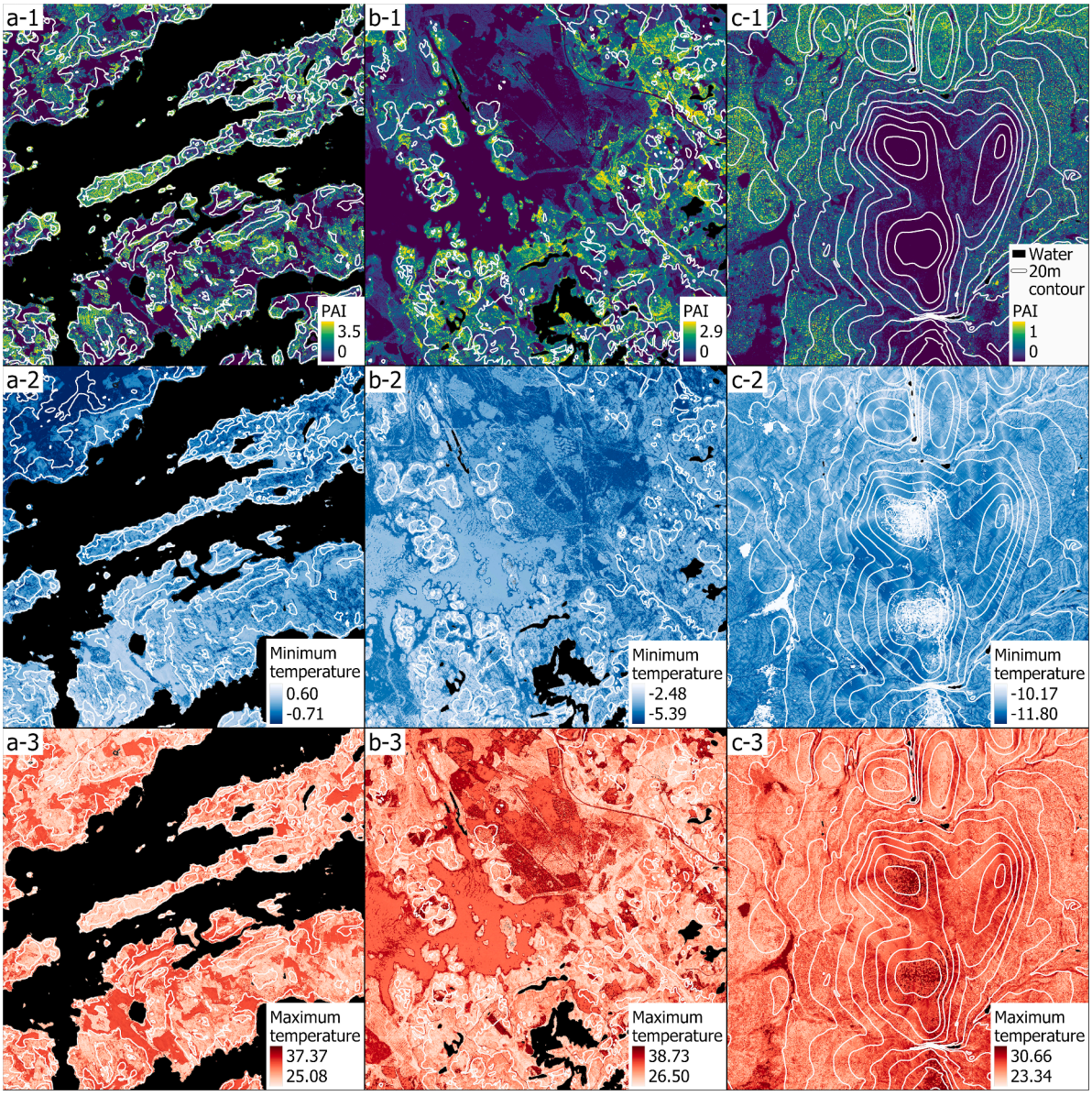

Fig. 5. The PAI (Plant Area Index) (1), modelled minimum (2) and maximum (3) temperatures from the KAR (Karkali, a), HYY (Hyytiälä, b) and VAR (Värriö, c) focus areas. Elevation is depicted by the white 20 m contour line for each area, while black areas depict water cover.

during the summer in the modelled temperatures. However, results suggest that there is a larger bias in maximum temperature predictions in the south facing sides of fell tops and minimum temperature predictions in the local topographic depressions where cold air pooling should lower temperatures further (Geiger, 1965). These fell dynamics can be greatly affected by the lack of a snow component in the model. The fell depressions could stay cooler for longer periods due to slower snow ablation than in other areas (Niittynen and Luoto, 2018), as could the northwest-facing sides compared to the southeast-facing ones. A generalization of the results is that the model performs best in areas with high PAI, taller trees, steeper North-West facing slopes with higher elevation than the surrounding area in this study setting.

4.2. Methodological limitations

There are multiple potential sources for differences in measured and modelled values, potentially deriving from the model itself, but also in the data and methodological limitations of this study. One of the known limitations is the rather coarse native resolution, or complete lack of, certain input variables. The most influential variable PAI was calculated from LiDAR data, but the national LiDAR dataset has a point density of 0.5 p/m^2. Lower LiDAR point densities have been found to lower the accuracy of forest variable estimations (such as tree height and stem volume) (e.g. Magnusson et al., 2007; Gobakken and Næsset, 2008). For example, a study conducted by Watt et al. (2014) showed an increase in the RMSE of tree height, volume and diameter estimations when point densities were thinned to 1 p/m^2 and lower. They also found that even point densities of 0.1 p/m^2 could give similar results as densities over 2 p/m^2 when used with higher accuracy DEM data. Due to the large extent of the focus areas in our study, producing higher point density LiDAR data using e.g., unmanned aerial vehicles was not feasible. However, there is currently ongoing production of a new, more accurate 5 p/m^2 national LiDAR dataset. From this, a more accurate DEM could be produced to be used even with the lower 0.5 p/m^2 LiDAR data and provide more detailed information about the vegetation structuring.

Missing vegetation and soil variables were estimated using either model tools or made homogenous over the focus areas. The soil classes used in *microclimf* are based on Aschonitis's and Antonopoulos's (2013)

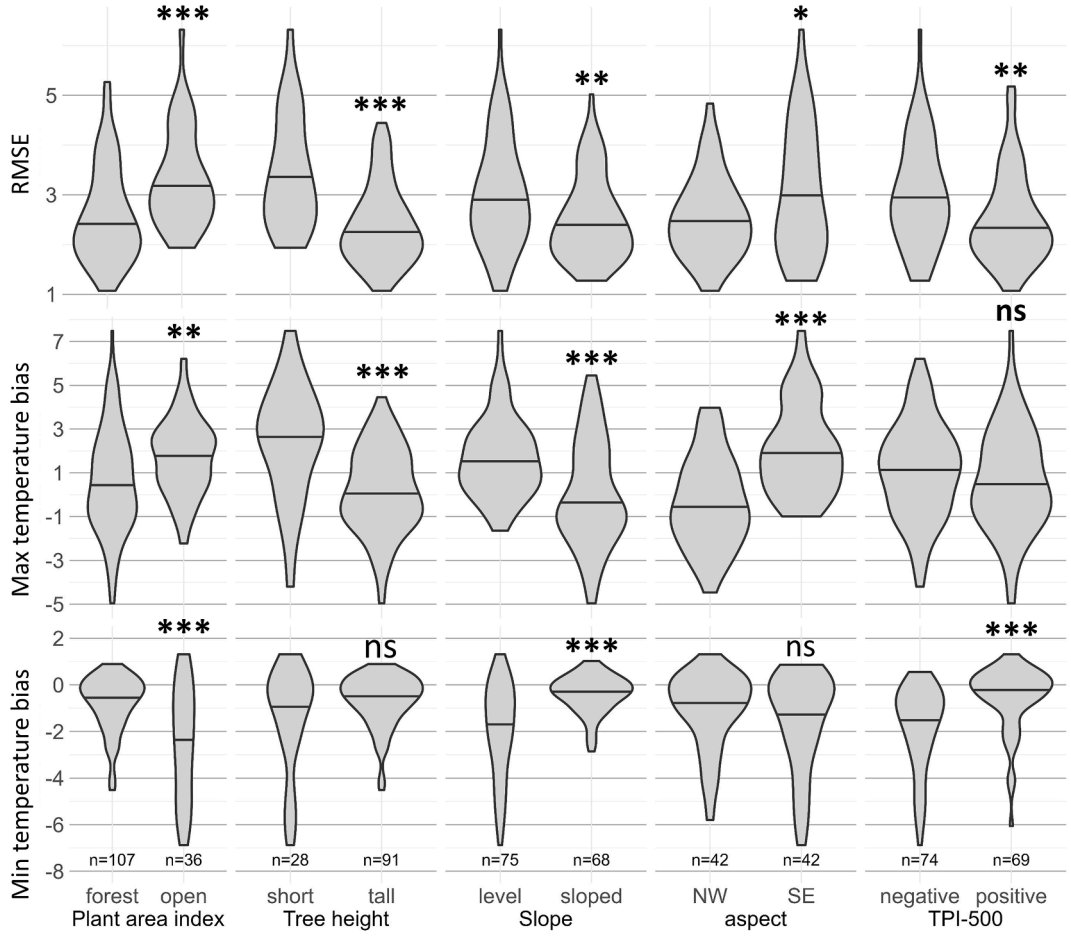

Fig. 6. Root Mean Square Error (RMSE) of three hourly measured and modelled temperatures and maximum (max) and minimum (min) temperature bias comparisons between forested (PAI > 0.1) and open (PAI < 0.1), short (< 10 m) and tall trees (>= 10 m), forested (PAI > 0.1) and open (PAI < 0.1), level (slope angle < 5 °) and sloped (slope angle >= 5 °), North-West (NW) and South-East (SE) facing slopes and negative and positive Topographic Position Index values at a 500 m radius (TPI-500). Black line depicts the 0.5 quartile. N value depicts the number of observations in each group. Statistical evaluation of the results was done with the Welch's two sample *t*-test and the level of significance is above the groups depicted as P ⟨ 0.001 = ***, $P < 0.01$ = **, $P < 0.05$ = * and P ⟩ 0.05 = ns (not significant).

soil type classifications and their parameters. For our focus areas, the available soil datasets, and their classifications do not meet the parameterization requirements presented by the model. This could be a key factor for the lower model performance in more open areas, where the soil type and radiation reflectance play a larger role in controlling the temperature dynamics at 15 cm height than in a closed canopy environment (Geiger, 1965). In addition, the model does not consider the different types of ground-level vegetation, which has been shown to be an important climate forcing factor for microclimate modelling (Stickley and Fraterrigo, 2021).

Another potential source for error is the uncertainties regarding microclimate measurements. The used Tomst loggers have an accuracy of 0.50 °C (Wild et al., 2019). Adding to this, the known issues of potential heating caused by radiation absorption by the logger itself (Maclean et al., 2021b) are likely causing significant bias to the maximum temperature comparisons between measured and modelled data. This may also be the reason for the outlier values in maximum temperatures (e.g., nearly 45 °C) in June – August months and a potential reason for the model consistently underestimated maximum temperatures in all sites. The loggers have also been shown to have a nocturnal minimum temperature bias, with the device underestimating temperatures in more open areas (Maclean et al., 2021b), which was also seen in the minimum temperature bias of our comparisons between open and forested measurement sites. This also likely explains the model's tendency to produce smaller temperature ranges compared to the measurement data in all areas (especially HYY and VAR).

4.3. *On the microclimate measurements and models*

Only recently have new local and regional microclimate observation networks, consisting of miniature loggers, helped to facilitate understanding of microclimatic variability across biomes (Wild et al., 2019; Lembrechts et al., 2020). Recent studies by Aalto et al. (2022) and Kemppinen et al. (2023) conducted across boreal and tundra landscapes in northern Europe quantified the remarkable spatiotemporal thermal-hydrological heterogeneity of these systems. Such large study designs of hundreds of microclimate stations are valuable for informing us about the magnitude of fine-scale climate variability. Large microclimate measurement datasets can also be used to develop empirical models, or used as in this study, as validation data for more mechanistic modelling approaches.

Mechanistic microclimate models are valuable tools in increasing our understanding of the different risks forest environments are facing under changing climate. For example, microclimate related phenomena, such as mapping and understanding species' microrefugia (Stickley and Fraterrigo, 2023), pest damages for trees (such as bark beetle) (Kautz et al., 2013), the transmission potential of arthropod vectors (Haider et al., 2017), alterations in snow dynamics and forest carbon sinks (e.g., Ahmed et al., 2021), and forest fire risk (Alexander, 2010) can be better understood and used for more informed decision making.

In this study, we found that the mechanistic model *microclimf* was able to predict the temperature dynamics over three focus areas in boreal forests. Acknowledging the limitations for some of the input variables, the results could benefit particularly from higher quality LiDAR and soil data. Currently, model applicability is mostly limited by the large range of input variables required, and the computational requirements for larger spatiotemporal extents with outputs of high spatial resolution. Here, we tested only the modelling of near-surface temperatures. In the future work, other model output variables, such as relative humidity and soil moisture would be important to validate for similar boreal forest environments. These could be used for more accurate drought risk estimations and recognizing potential fire ignition risk areas.

5. Conclusions

In this study, we modelled the near-surface microclimate temperature variation over a broad macroclimatic gradient, ranging from the deciduous forests of the hemiboreal area of Karkali, the large mires of the southern boreal area of Hyytiälä, and finally the open tundra summits in the northern boreal area of Värriö, using the spatially-resolved mechanistic microclimate model *microclimf*. We found that the model was able to predict temperature variability in each focus area and showed reasonable overall agreement between measured and modelled values at daily maximum, minimum and mean temperatures, along with instantaneous temperatures. The model was found to have the best performance in the hemiboreal area with dense canopy cover compared to the southern boreal area with extensive open landscapes and wetlands, and the northern boreal area with larger topographic variation and overall lower canopy coverage. Results reveal high spatiotemporal variability in the temperature ranges within each of the focus areas, demonstrating the high potential of mechanistic microclimate models to accurately predict temperature variability at high spatial and temporal resolution over boreal environments. In the future, new high spatiotemporal resolution microclimate data can be used both to factor in the actual microclimatic environment in different modelling systems and to increase our knowledge of the effects of land use and climate change on different environments and the species inhabiting them.

CRediT authorship contribution statement

Joonas Kolstela: Writing – review & editing, Writing – original draft, Visualization, Validation, Methodology, Formal analysis, Data curation, Conceptualization. **Tuomas Aakala:** Writing – review & editing, Supervision, Conceptualization. **Ilya Maclean:** Writing – review & editing, Validation, Software, Methodology. **Pekka Niittynen:** Writing – review & editing. **Julia Kemppinen:** Writing – review & editing. **Miska Luoto:** Writing – review & editing. **Tuuli Rissanen:** Writing – review & editing. **Vilna Tyystjärvi:** Writing – review & editing. **Hilppa Gregow:** Writing – review & editing. **Olli Vapalahti:** Writing – review & editing, Project administration. **Juha Aalto:** Writing – review & editing, Writing – original draft, Supervision, Methodology, Investigation, Conceptualization.

Declaration of competing interest

The authors declare that they have no known competing financial interests or personal relationships that could have appeared to influence the work reported in this paper.

Data availability

Generated microclimate data will be made available upon request. Validation data requests should be directed to the authors of https://doi.org/10.1016/j.agrformet.2022.109037

Acknowledgements

JK, HG, OV, JA acknowledges the funding by the Research Council of Finland Flagship funding (grant no. 337552), VECLIMIT project (grant no. 329323). The authors wish to acknowledge CSC – IT Center for Science, Finland, for computational resources.

Supplementary materials

Supplementary material associated with this article can be found, in the online version, at doi:10.1016/j.agrformet.2024.109995.

References

Aalto, J., Pirinen, P., Jylhä, K., 2016. New gridded daily climatology of Finland: permutation-based uncertainty estimates and temporal trends in climate. J. Geophys. Res. 121 (8) https://doi.org/10.1002/2015JD024651.

Aalto, J., Tyystjärvi, V., Niittynen, P., Kemppinen, J., Rissanen, T., Gregow, H., Luoto, M., 2022. Microclimate temperature variations from boreal forests to the tundra. Agric. For. Meteorol. 323 https://doi.org/10.1016/j.agrformet.2022.109037.

Ahmed, H.F., Helgason, W., Barr, A., Black, A., 2021. Characterization of spring thaw and its relationship with carbon uptake for different types of southern boreal forest. Agric. For. Meteorol. 307 https://doi.org/10.1016/j.agrformet.2021.108511.

Alexander, M.E., 2010. Surface fire spread potential in trembling aspen during summer in the boreal forest region of Canada. For. Chron. 86 (2) https://doi.org/10.5558/tfc86200-2.

Arnqvist, J., Freier, J., Dellwik, E., 2020. Robust processing of airborne laser scans to plant area density profiles. Biogeosciences 17 (23). https://doi.org/10.5194/bg-17-5939-2020.

Aschonitis, V.G., Antonopoulos, V.Z., 2013. New equations for the determination of soil saturated hydraulic conductivity using the van genuchten model parameters and effective porosity. Irrig. Drainage 62 (4). https://doi.org/10.1002/ird.1751.

Bradshaw, C.J.A., Warkentin, I.G., 2015. Global estimates of boreal forest carbon stocks and flux. Glob Planet Change 128. https://doi.org/10.1016/j.gloplacha.2015.02.004.

Bramer, I., Anderson, B.J., Bennie, J., Bladon, A.J., de Frenne, P., Hemming, D., Hill, R. A., Kearney, M.R., Körner, C., Korstjens, A.H., Lenoir, J., Maclean, I.M.D., Marsh, C. D., Morecroft, M.D., Ohlemüller, R., Slater, H.D., Suggitt, A.J., Zellweger, F., Gillingham, P.K, 2018. Advances in monitoring and modelling climate at ecologically relevant scales. Adv. Ecol. Res. 58 https://doi.org/10.1016/bs.aecr.2017.12.005.

De Frenne, P., Zellweger, F., Rodríguez-Sánchez, F., Scheffers, B.R., Hylander, K., Luoto, M., Vellend, M., Verheyen, K., Lenoir, J., 2019. Global buffering of temperatures under forest canopies. Nat. Ecol Evol. 3 (5) https://doi.org/10.1038/s41559-019-0842-1.

Dickinson, R.E., Henderson-Sellers, A., Kennedy, P.J., & Wilson, M.F. 1986. Biosphere-atmosphere Transfer Scheme (BATS) for the NCAR Community Climate Model. In Technical note, NCAR /TN-275+STR.

FAO. 2020. Global Forest Resources Assessment 2020: Main report. Rome. https://doi.org/10.4060/ca9825en.

Finnish Meteorological Institute. 2021. Ilmastovuosikatsaus 2020. (In Finnish) 10.35614/ISSN-2341-6408-IVK-2020-00.

Geiger, R., 1965. The Climate Near the Ground. Harvard University Press, Cambridge, Massachusetts. Print.

Gobakken, T., Næsset, E., 2008. Assessing effects of laser point density, ground sampling intensity, and field sample plot size on biophysical stand properties derived from airborne laser scanner data. Can. J. For. Res. 38 (5) https://doi.org/10.1139/X07-219.

Gonzalez, P., Neilson, R.P., Lenihan, J.M., Drapek, R.J., 2010. Global patterns in the vulnerability of ecosystems to vegetation shifts due to climate change. Glob. Ecol. Biogeogr. 19 (6) https://doi.org/10.1111/j.1466-8238.2010.00558.x.

Goudriaan, J., Waggoner, P.E., 1972. Simulating both aerial microclimate and soil temperature from observations above the foliar canopy. Netherlands J. Agric. Sci. 20 (2) https://doi.org/10.18174/njas.v20i2.17290.

Gril, E., Spicher, F., Greiser, C., Ashcroft, M.B., Pincebourde, S., Durrieu, S., Nicolas, M., Richard, B., Decocq, G., Marrec, R., Lenoir, J., 2023. Slope and equilibrium: a parsimonious and flexible approach to model microclimate. Methods Ecol. Evol. 14 (3) https://doi.org/10.1111/2041-210X.14048.

Haider, N., Kirkeby, C., Kristensen, B., Kjær, L.J., Sørensen, J.H., Bødker, R., 2017. Microclimatic temperatures increase the potential for vector-borne disease transmission in the Scandinavian climate. Sci. Rep. 7 (1) https://doi.org/10.1038/s41598-017-08514-9.

Harman, I.N., Finnigan, J.J., 2007. A simple unified theory for flow in the canopy and roughness sublayer. Boundary Layer Meteorol. 123 (2) https://doi.org/10.1007/s10546-006-9145-6.

Jokinen, P., Pirinen, P., Kaukoranta, J.P., Kangas, A., Alenius, P., Eriksson, P., Johansson, M., Wilkman, S., 2021. Tilastoja Suomen ilmastosta ja merestä 1991-2020. Ilmatieteen Laitos (In Finnish). http://hdl.handle.net/10138/336063.

Kautz, M., Schopf, R., Ohser, J., 2013. The "sun-effect": microclimatic alterations predispose forest edges to bark beetle infestations. Eur. J. For. Res. 132 (3), 453–465. https://doi.org/10.1007/s10342-013-0685-2.

Kearney, M.R., Porter, W.P., 2017. NicheMapR – an R package for biophysical modelling: the microclimate model. Ecography 40 (5). https://doi.org/10.1111/ecog.02360.
Kemppinen, J., Niittynen, P., Rissanen, T., Tyystjärvi, V., Aalto, J., Luoto, M., 2023. Soil moisture variations from boreal forests to the tundra. Water Resour. Res. 59 (6) https://doi.org/10.1029/2022WR032719.
Klinges, D.H., Duffy, J.P., Kearney, M.R., Maclean, I.M.D., 2022. mcera5: driving microclimate models with ERA5 global gridded climate data. Methods Ecol. Evol. 13 (7) https://doi.org/10.1111/2041-210X.13877.
Lembrechts, J.J., Lenoir, J., Roth, N., Hattab, T., Milbau, A., Haider, S., Pellissier, L., Pauchard, A., Ratier Backes, A., Dimarco, R.D., Nuñez, M.A., Aalto, J., Nijs, I., 2019. Comparing temperature data sources for use in species distribution models: from in-situ logging to remote sensing. Glob. Ecol. Biogeogr. 28 (11) https://doi.org/10.1111/geb.12974.
Lembrechts, J.J., Aalto, J., Ashcroft, M.B., de Frenne, P., Kopecký, M., Lenoir, J., Luoto, M., Maclean, I.M.D., Roupsard, O., Fuentes-Lillo, E., García, R.A., Pellissier, L., Pitteloud, C., Alatalo, J.M., Smith, S.W., Björk, R.G., Muffler, L., Ratier Backes, A., Cesarz, S., Nijs, I., 2020. SoilTemp: a global database of near-surface temperature. Glob. Chang. Biol. 26 (11) https://doi.org/10.1111/gcb.15123.
Lenoir, J., Graae, B.J., Aarrestad, P.A., Alsos, I.G., Armbruster, W.S., Austrheim, G., Bergendorff, C., Birks, H.J.B., Bråthen, K.A., Brunet, J., Bruun, H.H., Dahlberg, C.J., Decocq, G., Diekmann, M., Dynesius, M., Ejrnæs, R., Grytnes, J.A., Hylander, K., Klanderud, K., Svenning, J.C., 2013. Local temperatures inferred from plant communities suggest strong spatial buffering of climate warming across Northern Europe. Glob. Chang. Biol. 19 (5) https://doi.org/10.1111/gcb.12129.
Maclean, I.M.D., Mosedale, J.R., Bennie, J.J., 2019. Microclima: an r package for modelling meso- and microclimate. Methods Ecol. Evol. 10 (2) https://doi.org/10.1111/2041-210X.13093.
Maclean, I.M.D., Klinges, D.H., 2021a. Microclimc: a mechanistic model of above, below and within-canopy microclimate. Ecol. Modell. 451 https://doi.org/10.1016/j.ecolmodel.2021.109567.
Maclean, I.M.D., Duffy, J.P., Haesen, S., Govaert, S., de Frenne, P., Vanneste, T., Lenoir, J., Lembrechts, J.J., Rhodes, M.W., van Meerbeek, K., 2021b. On the measurement of microclimate. Methods Ecol. Evol. 12 (8) https://doi.org/10.1111/2041-210X.13627.
Maclean, I.M.D., & Klinges, D.H. 2023, October 20. Microclimf Github repository. https://github.com/ilyamaclean/microclimf.
Magnusson, M., Fransson, J.E.S., Holmgren, J., 2007. Effects on estimation accuracy of forest variables using different pulse density of laser data. Forest Sci. 53 (6).
Monteith, J.L. 1965. Evaporation and environment. In Symposia of the Society for Experimental Biology (Vol. 19).
Määttänen, A.M., Virkkala, R., Leikola, N., Aalto, J., Heikkinen, R.K., 2023. Combined threats of climate change and land use to boreal protected areas with red-listed forest species in Finland. Glob. Ecol. Conserv. 41. https://doi.org/10.1016/j.gecco.2022.e02348.
Niittynen, P., Luoto, M., 2018. The importance of snow in species distribution models of arctic vegetation. Ecography 41 (6). https://doi.org/10.1111/ecog.03348.
Ogée, J., Brunet, Y., Loustau, D., Berbigier, P., Delzon, S., 2003. MuSICA, a CO2, water and energy multilayer, multileaf pine forest model: evaluation from hourly to yearly time scales and sensitivity analysis. Glob. Chang. Biol. 9 (5), 697–717. https://doi.org/10.1046/j.1365-2486.2003.00628.x.
Penman, H.L., 1948. Natural evaporation from open water, bare soil and grass. Proc. R. Soc. Lond. A Math. Phys. Sci. 193 (1032).
Pohjanmies, T., Triviño, M., le Tortorec, E., Mazziotta, A., Snäll, T., Mönkkönen, M., 2017. Impacts of forestry on boreal forests: an ecosystem services perspective. In Ambio 46 (7). https://doi.org/10.1007/s13280-017-0919-5.
Porter, W.P., Mitchell, J.W., Beckman, W.A., DeWitt, C.B., 1973. Behavioral implications of mechanistic ecology. Oecologia 13 (1). https://doi.org/10.1007/bf00379617.
R Core Team, 2022. 2020. R: a language and environment for statistical computing. R Foundation for Statistical Computing. Vienna, Austria.
Raupach, M.R., 1987. A lagrangian analysis of scalar transfer in vegetation canopies. Q. J. R. Meteorol. Soc. 113 (475) https://doi.org/10.1002/qj.49711347507.
Raupach, M.R., 1994. Simplified expressions for vegetation roughness length and zero-plane displacement as functions of canopy height and area index. Boundary-Layer Meteorol. 71 (1–2) https://doi.org/10.1007/BF00709229.
Renaud, V., Innes, J.L., Dobbertin, M., Rebetez, M., 2011. Comparison between open-site and below-canopy climatic conditions in Switzerland for different types of forests over 10 years (1998-2007). Theor. Appl. Climatol. 105 (1) https://doi.org/10.1007/s00704-010-0361-0.
Saarikoski, H., Jax, K., Harrison, P.A., Primmer, E., Barton, D.N., Mononen, L., Vihervaara, P., Furman, E., 2015. Exploring operational ecosystem service definitions: the case of boreal forests. Ecosyst. Serv. 14 https://doi.org/10.1016/j.ecoser.2015.03.006.
Samuelsson, P., Kourzeneva, E., Mironov, D., 2010. The impact of lakes on the European climate as simulated by a regional climate model. Boreal Environ. Res. 15 (2).
Stickley, S.F., Fraterrigo, J.M., 2021. Understory vegetation contributes to microclimatic buffering of near-surface temperatures in temperate deciduous forests. Landsc. Ecol. 36 (4) https://doi.org/10.1007/s10980-021-01195-w.
Stickley, S.F., Fraterrigo, J.M., 2023. Microclimate species distribution models estimate lower levels of climate-related habitat loss for salamanders. J. Nat. Conserv. 72 https://doi.org/10.1016/j.jnc.2023.126333.
Thom, D., Sommerfeld, A., Sebald, J., Hagge, J., Müller, J., Seidl, R., 2020. Effects of disturbance patterns and deadwood on the microclimate in European beech forests. Agric. For. Meteorol. 291 https://doi.org/10.1016/j.agrformet.2020.108066.
van Wagner, C.E., 1974. Structure of the Canadian forest fire weather index. Depart. Environ. Can. Forest. Serv. Publ. 1333.
Venäläinen, A., Heikinheimo, M., 2003. The Finnish forest fire index calculation system. Early Warning Syst. Nat. Dis. Reduct. https://doi.org/10.1007/978-3-642-55903-7_88.
Venäläinen, A., Lehtonen, I., Laapas, M., Ruosteenoja, K., Tikkanen, O.P., Viiri, H., Ikonen, V.P., Peltola, H., 2020. Climate change induces multiple risks to boreal forests and forestry in Finland: a literature review. Glob. Chang. Biol. 26 (8) https://doi.org/10.1111/gcb.15183.
Watt, M.S., Meredith, A., Watt, P., Gunn, A., 2014. The influence of LiDAR pulse density on the precision of inventory metrics in young unthinned Douglas-fir stands during initial and subsequent LiDAR acquisitions. N. Z. J. For. Sci. 44 (1) https://doi.org/10.1186/s40490-014-0018-3.
Wen, L., Lv, S., Li, Z., Zhao, L., Nagabhatla, N., 2015. Impacts of the two biggest lakes on local temperature and precipitation in the Yellow River source region of the Tibetan Plateau. Adv. Meteorol. https://doi.org/10.1155/2015/248031, 2015.
Wild, J., Kopecký, M., Macek, M., Šanda, M., Jankovec, J., Haase, T., 2019. Climate at ecologically relevant scales: a new temperature and soil moisture logger for long-term microclimate measurement. Agric. For. Meteorol. 268 https://doi.org/10.1016/j.agrformet.2018.12.018.
Yu, L., Liu, T., 2019. The impact of artificial wetland expansion on local temperature in the growing season-the case study of the Sanjiang Plain, China. Remote Sens. 11 (24) https://doi.org/10.3390/rs11242915.
Yuan, H., Dai, Y., Dickinson, R.E., Pinty, B., Shangguan, W., Zhang, S., Wang, L., Zhu, S., 2017. Reexamination and further development of two-stream canopy radiative transfer models for global land modeling. J. Adv. Model. Earth Syst. 9 (1) https://doi.org/10.1002/2016MS000773.